中国激光

纳米颗粒对2195铝锂合金激光焊微观组织的影响

占小红[1*]，李悦[1]，赵艳秋[1]，王建峰[1]，高雪松[2]，周军[2]

[1]南京航空航天大学材料科学与技术学院，江苏 南京 211106；

[2]南京先进激光技术研究院，江苏 南京 211106

摘要　基于航空航天器轻量化、高性能及高可靠性的制造要求，为增加焊缝强化相数量、获得高质量平板对接结构，采用填充4047焊丝和2319纳米焊丝的激光焊接方法对2 mm厚的2195铝锂合金对接结构进行焊接。针对填充不同焊丝得到的焊接接头微观组织、元素含量及力学性能进行对比分析。结果表明，激光填丝焊接相较于激光自熔焊，焊缝组织得到细化，填充2319纳米焊丝的激光焊接焊缝组织均为细小的等轴晶，纳米颗粒的添加促进了柱状晶向等轴晶的转变。同时，纳米焊丝熔化后进入激光焊接熔池，有效补充了焊缝的元素烧损，含Cu强化相增加。因此，填充4047焊丝的激光焊接接头的抗拉强度为259.9 MPa，相较于无填充焊丝的激光自熔焊提高了17.07%；填充纳米焊丝的激光焊接接头的抗拉强度达到253.51 MPa，相比于激光自熔焊提高了14.19%。填充4047焊丝能有效提高2195铝锂合金激光焊接焊缝的抗拉强度。

关键词　激光技术；激光焊接；铝锂合金；等轴晶；纳米焊丝；微观组织

中图分类号　TG456.7　　　**文献标志码**　A　　　**DOI**：10.3788/CJL221337

1　引　　言

作为我国新一代航天器贮箱结构的备选材料，铝锂合金自20世纪50—60年代起，为航空航天领域相关结构件的减重作出了重要贡献[1-2]。铝合金中添加了最轻的合金元素锂(Li)，可以在大幅度减小密度的同时提高刚度[3]。研究表明，每增加一个单位锂元素能够实现材料质量减重5%，强度增加30%[4-5]。而航天器结构质量的减重意味着其运载的有效载荷增加，每千克有效载荷可带来4400~110000美元的经济效益[6]。

高强度的2195铝锂合金在室温和低温下具有优异的强度和断裂韧性，主要应用于航天运载火箭的低温贮箱，满足航空航天领域关键结构的减重需求[7-8]。而在制造2195铝锂合金航天器贮箱结构件方面，铆接技术存在效率低、无法进一步减重、成本高等缺点，国内外研究学者转向了焊接技术，主要集中于电弧焊接、搅拌摩擦焊和电子束焊三种方法，关于激光焊接方法的研究较少[9-10]。而激光焊接技术作为一种高能束连接方法，具有能量密度高、焊接质量好、精度高、生产效率高、减重效果好等特点，能够很好解决上述问题[11]。因此在航天器贮箱结构的生产方面，激光焊接是此类材料和结构的理想连接技术[12-13]。

合金元素影响铝合金中析出物的种类、尺寸、体积分数和分布形态，而析出物和显微组织决定铝合金的力学性能。因此，对于如何改善2195铝锂合金焊态下接头的物相成分，以提高接头性能，这是值得深入研究的一个课题。张心怡[14]研究了填充Al-Mg和Al-Si焊丝的2060铝锂合金激光焊接头抗拉强度，研究结果表明，填充Al-Mg焊丝后焊缝Mg元素得到补充，晶界和枝晶间生成大量T2相(Al_6CuLi_3)；填充Al-Si焊丝后晶界和枝晶间生成大量T相(AlLiSi)和θ相(Al_2Cu)。刘强[15]针对5 mm厚5A01铝合金开展了激光活性焊接实验，研究其对焊缝中镁元素含量的影响，发现添加活性剂后焊缝未检测出新的元素成分和物相组成，且相比于活性剂，焊接参数对镁元素烧损量的影响更大。林凯莉等[16]开展了填充4047焊丝2195铝锂合金激光焊接实验，发现4047焊丝提供了大量Al-Si共晶物，有效降低了接头裂纹倾向，同时适当降低焊接速度可以减少低熔点共晶物的产生，有利于抑制裂纹产生。栗卓新等[17]发现，在焊缝中填加纳米陶瓷颗粒可细化晶粒，减少焊接缺陷，并起到强化焊缝的作用。目前，国内外关于填充纳米焊丝对铝锂合金激光焊接组织与性能的影响未有报道。

因此，本文通过填充4047焊丝和2319纳米焊丝，开展了2195铝锂合金激光焊接实验，对比分析了不同填充元素对激光焊接焊缝微观组织、合金元素分布以及力学性能的影响。

收稿日期：2022-10-18；**修回日期**：2022-11-18；**录用日期**：2022-11-24；**网络首发日期**：2022-12-04

基金项目：中央高校基本科研业务费专项资金(NF2022003，NS2022062)

通信作者：*xiaohongzhan_nuaa@126.com

2 实验材料与方法

2.1 实验材料与方法

针对2195铝锂合金开展了激光焊接及激光填丝焊接实验研究。本实验采用的焊件尺寸为100 mm×50 mm×2 mm，不开坡口，其三维几何结构如图1(a)所示。焊丝选取直径为1.2 mm的4047焊丝以及直径为1.2 mm、含2%(质量分数)TiC颗粒的2319纳米焊丝，具体的化学成分如表1所示。如图2所示，2319纳米焊丝含有TiC纳米颗粒，其中SEM为扫描电镜。

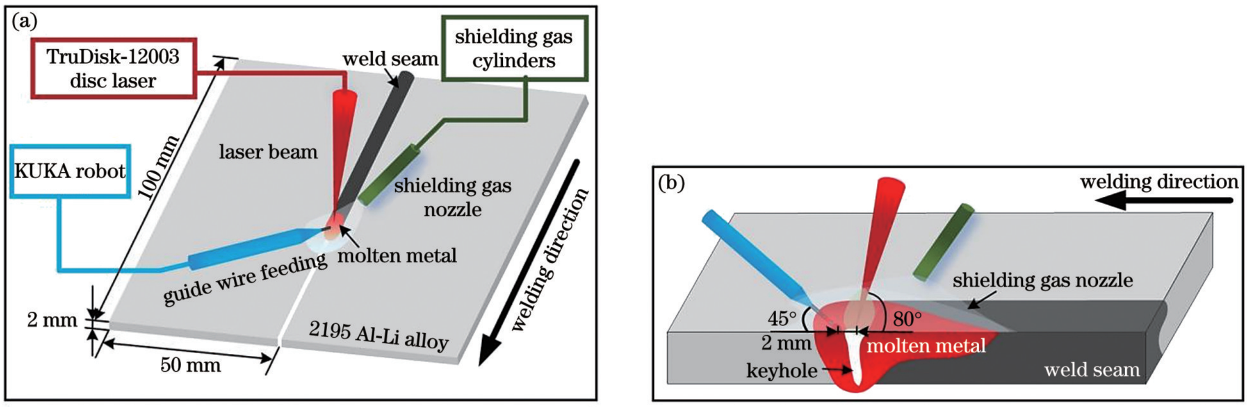

图1 激光焊接示意图。(a)激光填丝焊；(b)熔池形貌

Fig. 1 Schematics of laser welding. (a) Laser welding with filling wire; (b) molten pool morphology

表1 2195铝锂合金、4047焊丝及2319纳米焊丝的主要化学成分(质量分数，%)

Table 1 Main chemical compositions of 2195 Al-Li alloy, 4047 filler wire, and 2319 filler wire (mass fraction, %)

Element	Li	Cu	Mg	Zr	Ag	Zn	Mn	Si	Fe	Cr	Ti	V	TiC	Al
2195	1.10	4.00	0.40	0.11	0.40	≤0.25	≤0.25	–	–	–	–	–	–	Bal.
4047 filler wire	–	0.0300	0.1000	–	–	0.2000	0.1500	12.0000	0.8000	0.0500	0.0025	–	–	Bal.
2319 filler wire	–	5.600	0.200	–	–	0.100	0.300	0.200	0.300	–	0.150	0.100	2.000	Bal.

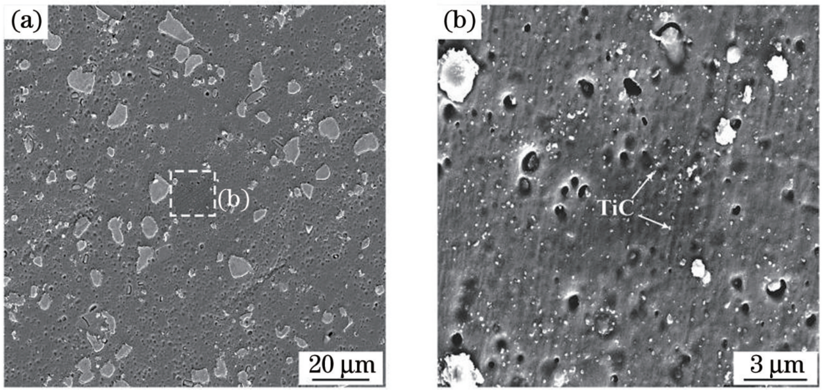

图2 含TiC纳米颗粒的2319纳米焊丝的SEM图。(a)形貌；(b)TiC纳米颗粒

Fig. 2 SEM images of TiC nanoparticle-reinforced 2319 filler wire. (a) Morphology; (b) TiC nanoparticles

2.2 实验设备与方法

2195铝锂合金激光焊接实验采用的实验设备如图3所示，铝锂合金激光填丝焊接采用碟片式激光器，其激光功率最高可达到12000 W。激光焊接通过六轴机器人实现，采用专用焊接工装夹具实现试样的装夹固定。填丝焊接通过送丝机实现送丝，送丝嘴与激光工作头夹角为45°。

激光功率为2.5 kW，焊接速度为1.5 m/min，离焦量为0 mm。设置激光束与工件之间的夹角为80°，保护气采用氩气，其流量为15 L/min。铝锂合金平板对接激光填丝焊接实验过程如图1(b)所示，实验采用0.2 mm的装配间隙。送丝速度为3 m/min。考虑到光丝间距对熔池稳定性具有显著影响，设置光丝间距为2 mm。由于铝合金表面容易生成一层具有吸湿性的致密氧化膜，因此对试样进行打磨和烘干处理，去除表面氧化膜和水蒸气，使试样表面无污染物并呈现金属光泽，在减少激光反射作用的同时防止焊缝中形成气孔、裂纹等焊接缺陷。

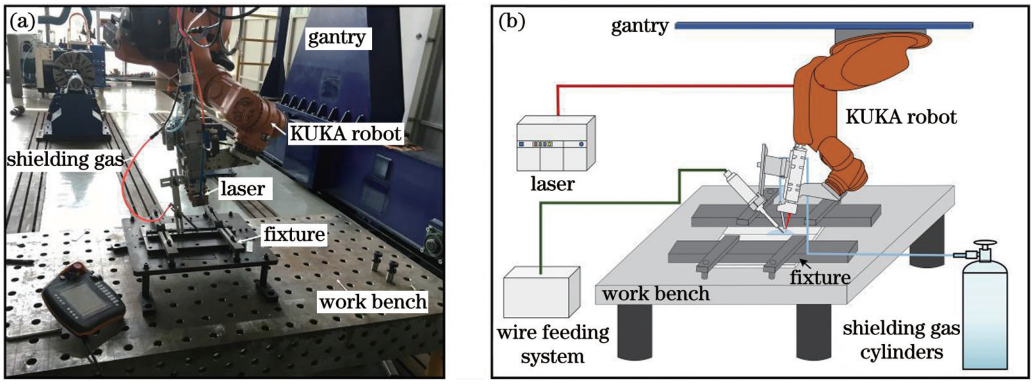

图 3　激光填丝焊接设备。(a)实物图;(b)示意图

Fig. 3　Laser wire filling welding equipment. (a) Physical map; (b) schematic

3　分析与讨论

3.1　微观组织分析

图 4 所示为铝锂合金激光自熔焊焊接接头微观组织。可以看到试样完全焊透,接头横截面中没有出现明显焊接缺陷。选取接头不同区域进行组织形貌观察,2195 铝锂合金焊缝微观组织由靠近熔合线处的等轴细晶区(EQZ)、柱状晶区和中心树枝晶区组成。熔合线处焊缝组织出现 EQZ,这是由于合金中存在 Zr 元素和 Li 元素,Zr 元素能够形成高熔点金属间化合物 Al_3Zr,在熔池中不会被熔化从而成为异质形核的质点[18];Li 元素可以降低吉布斯自由能,增加过冷度,从而提高异质形核率,细化晶粒。在这两种元素的作用下,最终在熔合线处焊缝区形成 EQZ,其中熔合线处焊缝区中部位置的 EQZ 范围较大。此外,在垂直于焊接熔池边界的方向上,散热最快、温度梯度最大,因此晶粒生长方向为最优的结晶生长方向,从熔合线到焊缝中心,基于所形成的 EQZ 表面形成柱状晶。而在焊缝中心,由于散热条件变差、温度梯度减小,同时晶粒结晶速度加快,因此焊缝金属的生长方式发生转变,在熔池中形成等轴树枝晶。

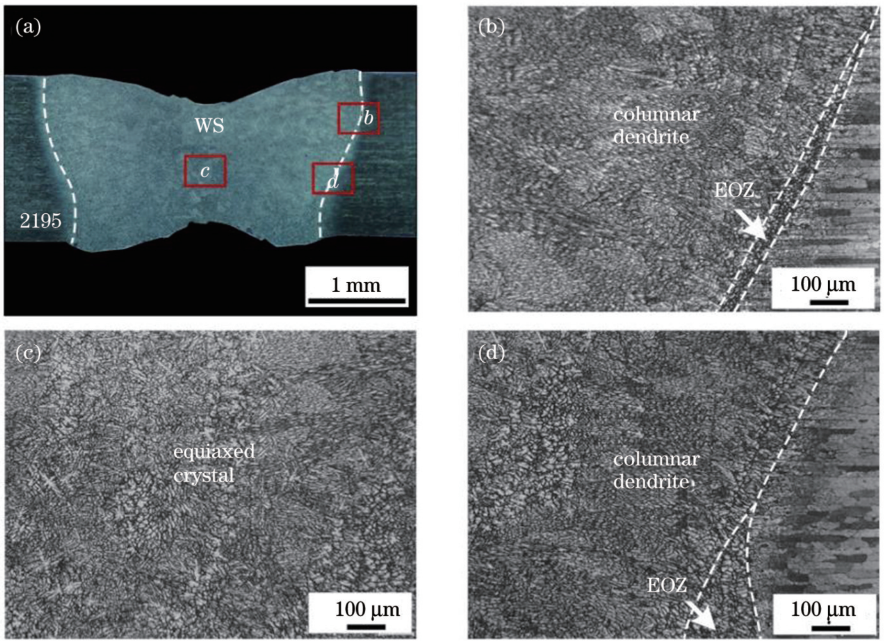

图 4　激光自熔焊焊接接头不同区域的微观组织。(a)宏观形貌;(b)焊缝右上角;(c)焊缝中心;(d)焊缝右下角

Fig. 4　Microstructures of laser self-melting welded joint in different areas. (a) Macro morphology; (b) upper right corner of weld; (c) center of weld; (d) bottom right corner of weld

图 5 所示为填充 4047 焊丝的典型焊缝微观组织形貌。分析其在激光焊接热作用下的分布规律,可以明显观察到等轴细晶区与柱状晶区的过渡位置,焊缝中部等轴细晶区最窄,焊缝顶部和底部等轴细晶区较宽。靠近熔合线处为等轴细晶区,向焊缝中心方向为柱状晶区,焊缝中心为树枝晶区。与激光自熔焊的焊缝组织相比,填充 4047 焊丝焊缝的等轴细晶区更窄,晶粒更加细小;柱状晶区域同样更窄,晶粒更细长;中心树枝晶区更宽且组织致密,等轴树枝晶与粗大树枝晶混合分布。填充 4047 焊丝可以促进焊缝显微组织细化,

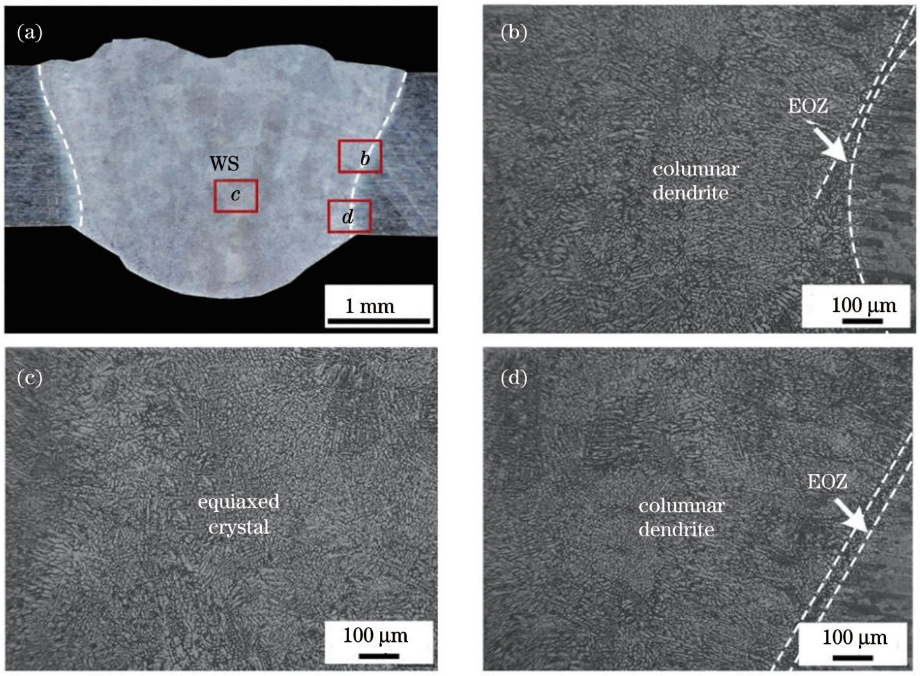

图5　填充4047焊丝激光焊接接头不同区域的微观组织。(a)宏观形貌;(b)焊缝右上角;(c)焊缝中心;(d)焊缝右下角

Fig. 5　Microstructures of joint by laser wire filling welding with 4047 in different areas. (a) Macro morphology; (b) upper right corner of weld; (c) center of weld; (d) bottom right corner of weld

但并未得到组织分布均匀的焊缝,中心区域粗大树枝晶呈簇状聚集在等轴树枝晶外围,且出现了二次枝晶比较发达的树枝晶。

图6所示为填充2319纳米焊丝的典型焊缝微观组织分布规律。与激光自熔焊和填充4047焊丝的横截面形貌相比,填充2319纳米焊丝的焊缝横截面各区域微观组织过渡并不明显,从横截面宏观形貌仅能观察到焊缝与热影响区的明显边界。靠近熔合线处为等轴细晶区,向焊缝中心方向延伸为等轴树枝晶区,未观察到明显的柱状晶区。纳米颗粒的存在促进了柱状晶向等轴晶的转变,晶粒得到细化[19]。研究认为,填充2319纳米焊丝焊缝树枝晶的枝晶臂简单,2319纳米焊丝不仅可以促进焊缝显微组织细化[20],还可得到组织分布均匀的焊缝。

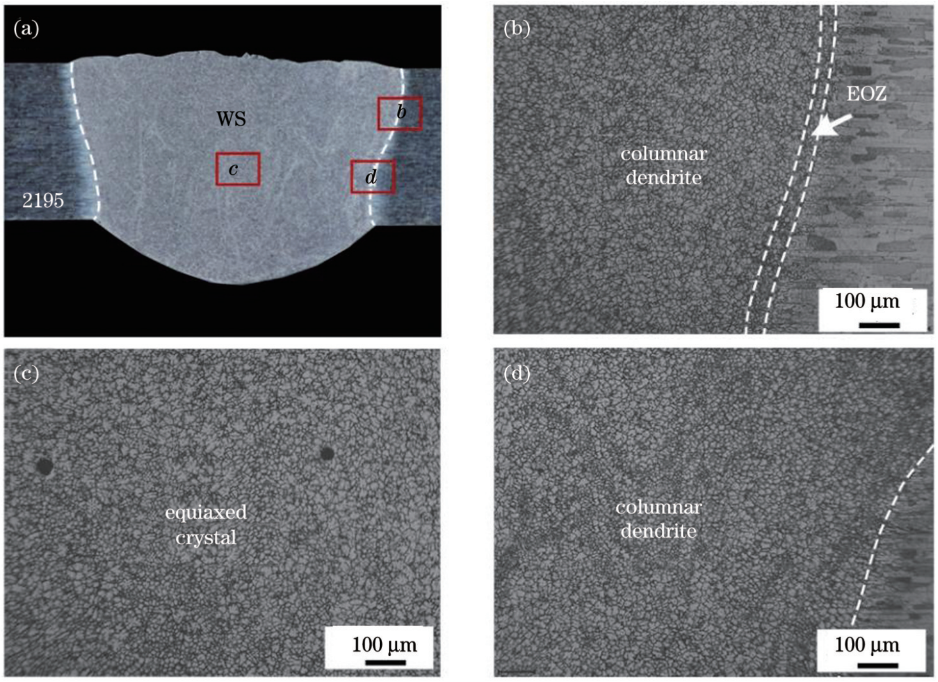

图6　填充2319纳米焊丝激光焊接接头不同区域的微观组织。(a)宏观形貌;(b)焊缝右上角;(c)焊缝中心;(d)焊缝右下角

Fig. 6　Microstructures of joint by laser wire filling welding with 2319 in different areas. (a) Macro morphology; (b) upper right corner of weld; (c) center of weld; (d) bottom right corner of weld

如图7所示，相比于相同参数下自熔焊的焊缝横截面形貌，填充焊丝焊缝横截面上的熔宽和焊缝面积均增加，可以发现，2319纳米焊丝焊缝横截面面积更大。这是由于2319纳米焊丝含有纳米颗粒，熔池流动性更好，能够及时补充焊缝烧损金属。

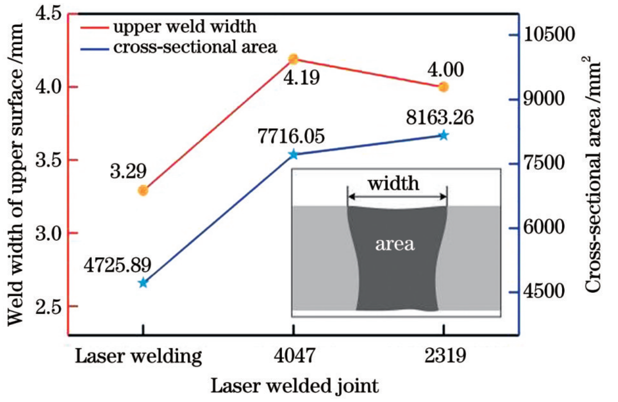

图7　激光焊接接头的上表面熔宽和焊缝横截面积

Fig. 7　Weld width of upper surface and cross-sectional area of laser welded joint

如图8所示，2195铝锂合金激光自熔焊接头组织从熔合线处到焊缝中心的演变大致依次表现为等轴细晶区、柱状晶区和等轴树枝晶区，而2319纳米焊丝激光焊接接头的组织从熔合线处到焊缝中心的演变大致依次表现为等轴细晶区、等轴树枝晶。2319纳米焊丝激光焊接接头整体晶粒尺寸更小，枝晶臂更简单。TiC颗粒弥散分布在熔池中能够大幅度降低体系自由能，从而克服了晶核在颗粒表面的形核能垒。晶核在熔合线区形核的同时，由于TiC颗粒的加入产生低的形核体系自由能，熔合线附近的TiC颗粒表面开始形核。熔池中晶粒形状及尺寸由形核过冷的大小决定，极低的形核过冷可抑制柱状晶的生长。同时，TiC颗粒的加入使得熔池中心增加了形核点，柱状晶的生长空间被大幅度压缩。此外，分布在晶界区的TiC颗粒阻碍晶界迁移，同样使得柱状晶的生长被抑制。低的凝固速率为枝晶的粗化提供了时间，从而促进柱枝晶向等轴晶的转变。

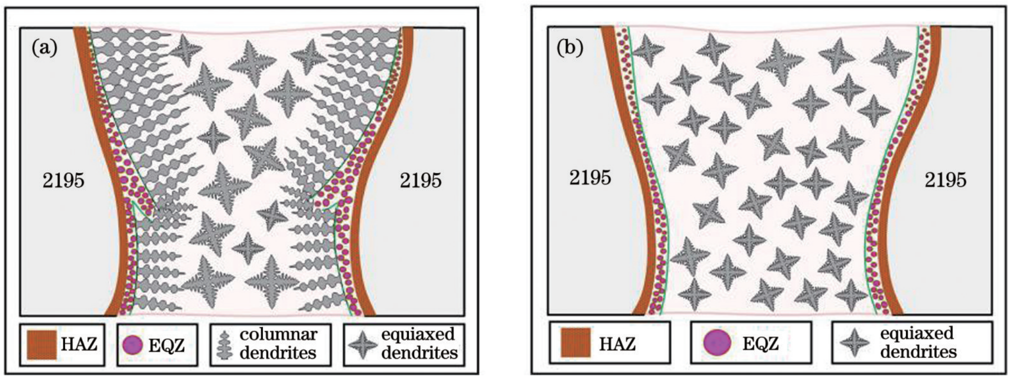

图8　激光焊接接头上熔宽和焊缝面积。(a)激光自熔焊；(b)填充2319纳米焊丝激光焊

Fig. 8　Weld width of upper surface and cross-sectional area of laser welded joint. (a) Laser self-melting welding; (b) laser wire filling welding with 2319

3.2　元素分布分析

为了进一步定量分析不同焊接方式下晶粒内部和晶界析出相的元素含量，对EQZ内部和晶界析出相分别进行了点扫描。表2为激光自熔焊下2195铝锂合金焊接接头EQZ的元素分布。Al元素在晶粒内部含量较多，在晶界析出相中的含量较少；Cu元素、Mg元素和Si元素在晶粒内部含量较少，在晶界析出相中的含量较多。

表2　激光自熔焊 EQZ 元素能谱结果

Table 2　Energy spectrum results of EQZ elements in laser self-melting welding

Position	Al mass fraction /%	Cu mass fraction /%	Mg mass fraction /%	Si mass fraction /%
Grain interior	72.48	7.12	0.61	0.31
Grain boundary precipitate	48.78	25.93	0.83	0.60

表3所示为焊丝4047填充下2195铝锂合金激光焊接接头EQZ的元素分布，Mg元素在晶粒内部含量稍高于晶界析出相含量，含量差别不大。同时，Si元素在晶粒内部含量大大低于晶界析出相含量。4047焊

表3　4047 焊丝激光焊接 EQZ 元素能谱结果

Table 3　Energy spectrum results of EQZ elements in laser welding with 4047 welding wire

Postion	Al mass fraction /%	Cu mass fraction /%	Mg mass fraction /%	Si mass fraction /%
Grain interior	87.81	3.3	0.95	0.87
Grain boundary precipitate	71.63	6.39	0.68	13.21

丝中Si元素含量较高，在焊接过程中进入到熔池，析出相可能为Mg_2Si相、Si相或者Si的二元共晶，对强度影响较小，但是对合金的塑性和断裂韧性影响较大。晶粒内部Cu元素含量较低，析出相内Cu元素含量较高，析出相为富Cu相。

表4为2319纳米焊丝填充下2195铝锂合金激光焊接接头EQZ的元素分布。相较于晶粒内部，Al元素在晶界析出相中的含量较少，Cu、Si、Mg元素在晶界处聚集，属于典型的晶界偏析。特别地，Cu元素在晶粒内部和晶界析出相中的含量差别很大，晶界偏析严重。

表4　2319纳米焊丝激光焊接EQZ元素能谱结果

Table 4　Energy spectrum results of EQZ elements in laser welding with 2319 filler wire

Position	Al mass fraction /%	Cu mass fraction /%	Mg mass fraction /%	Si mass fraction /%
Grain interior	90.64	2.53	0.83	0.48
Grain boundary precipitate	59.35	30.45	1.70	1.28

激光填丝焊缝中的Cu元素含量、烧损率和补充率如表5所示，在相同的工艺参数下，填充4047焊丝时Cu元素烧损率提高了一倍。由于2319纳米焊丝中Cu元素含量较高，因此焊接过程中Cu元素得到了大量补充，最终焊缝中元素含量高于母材。

表5　激光填丝焊缝中Cu元素含量

Table 5　Cu element contents in weld by laser welding with filling wire

Condition	Mass fraction of Cu element /%	Element burnout rate /%	Element replenishment rate /%
Base metal	4.00	–	–
Laser welding without wire filling	3.40	15.00	–
Laser welding with 4047 filler wire	2.76	31.00	–
Laser welding with 2319 filler wire	4.26	–	6.50

由以上分析可知，焊缝中主要合金元素为Al元素、Cu元素和Mg元素，在焊缝形成的过程中发生了元素的重新分布，Al元素主要聚集在晶粒内部，Cu元素主要聚集在晶界处，Mg元素分布较为均匀。对比有无填充2319纳米焊丝，可以发现填充2319纳米焊丝激光焊接焊缝晶粒内部Al元素含量显著增加，Cu元素减少；晶界处分布着大量的Cu元素，Cu元素得到补充，含Cu强化相增加。

3.3　拉伸性能分析

针对有无填充焊丝激光焊接获得的2195铝锂合金焊接接头开展拉伸实验，结果如图9所示。同时，也测得母材的拉伸强度为446 MPa。与母材本身的力学性能相比，焊接接头的拉伸强度均有一定程度的降低。在拉伸过程中，所有接头断裂均发生在焊缝处。与接头热影响区和母材相比，焊缝为接头的薄弱区。可以看出，与不填充纳米焊丝相比，填充纳米焊丝后接头的力学性能得到了显著改善，激光自熔焊焊接接头抗拉强度为222.01 MPa，断后延伸率为2.51%，填充4047焊丝的激光焊接接头拉伸强度高于填充2319纳米焊丝的激光焊接接头抗拉强度，填充4047焊丝的激光焊接接头抗拉强度为259.9 MPa，相较于无填充焊丝的焊接接头抗拉强度提高了17.07%，断后延伸率为1.8%；填充2319纳米焊丝的激光焊接接头抗拉强度为253.51 MPa，断后延伸率为2.6%，抗拉强度提高了14.19%。填充4047焊丝的激光焊接接头拉伸强度高于填充2319纳米焊丝的激光焊接接头。其原因为4047焊丝含有大量的Si元素，提高了接头强度，而2319纳米焊丝虽然有利于获得均匀的焊缝组织，但其补充的Cu元素在焊缝中形成亚稳相θ'相（Al_2Cu）及T1相（Al_2CuLi），T1相能够阻止位错运动，提高合金强度，但该相强化效果较弱。

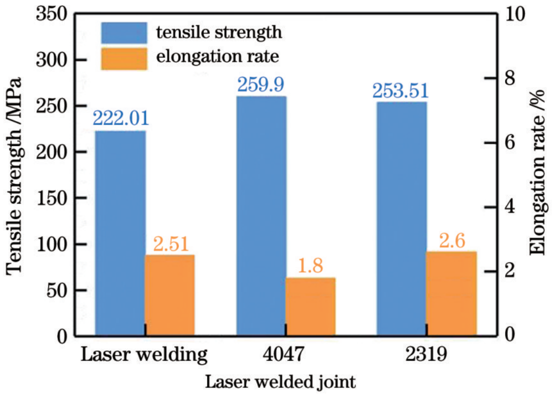

图9　不同焊接方式下激光焊接接头抗拉强度与伸长率

Fig. 9　Tensile strength values and elongation rates of laser welded joints under different welding methods

对有无填充焊丝的激光焊接接头拉伸实验断口进行SEM观察，如图10所示。可以看出，三组试样的断口同样呈现典型的韧窝特征，其断裂机制为微孔聚集断裂。对比不同填充材料下试样拉伸断口呈现的韧窝特征，可以观察到填充2319纳米焊丝试样的拉伸断口

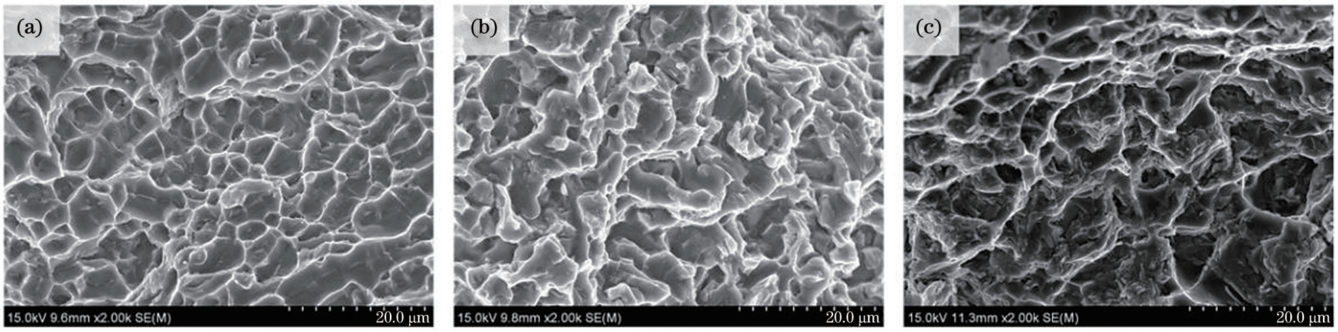

图 10 激光焊接接头拉伸断口形貌。(a)激光自熔焊;(b)填充 4047 焊丝;(c)填充 2319 纳米焊丝

Fig. 10 Fracture morphologies of laser welded joints during tensile testing. (a) Laser welding; (b) laser welding with 4047 filler wire; (c) laser welding with 2319 filler wire

中的韧窝形状更大,并且在韧窝底部观察到了不规则且较深的孔隙。2319 纳米焊丝可以促进熔池流动,增大了焊缝中气孔产生的可能性,因此该种填充材料下得到的试样更容易产生气孔,在试样断裂的过程中气孔易成为裂纹的扩展源,从而降低了接头的力学性能。

4 结 论

采用不同的焊丝实现了铝锂合金的激光焊接。通过对比 2195 铝锂合金激光自熔焊以及激光填丝焊接接头,发现自熔焊和填充 4047 焊丝激光焊接接头的焊缝区域组织由等轴细晶、柱状晶和等轴树枝晶组成;填充 2319 纳米焊丝的激光焊接接头焊缝区域由等轴细晶和等轴树枝晶组成。相较于激光自熔焊,填充 2319 纳米焊丝焊缝晶界处分布着大量的 Cu 元素,Cu 元素补充率达到 6.5%。填充 4047 焊丝时,2195 铝锂合金激光焊接过程中 Si 元素得到补充,焊缝组织晶界处分布大量的 Si 元素,含 Si 强化相增加。激光填充焊相比于激光自熔焊,能量作用更剧烈,Li 元素烧损更加严重。填充 4047 焊丝和 2319 纳米焊丝均对 2195 铝锂合金激光焊接接头的抗拉强度有提高作用。填充 4047 焊丝的激光焊接接头抗拉强度为 259.9 MPa,相较于无填充焊丝的焊接接头抗拉强度提高了 17.07%,填充纳米焊丝的 2195 铝锂合金激光焊接接头的抗拉强度为 253.51 MPa,相较于激光自熔焊提高了 14.19%,拉伸强度相差不大。但填充 4047 焊丝的激光焊接接头的延伸率为 1.8%,填充纳米焊丝的 2195 铝锂合金激光焊接接头的断后延伸率为 2.6%,比激光自熔焊接头的延伸率低。因此,相较于 4047 焊丝,2319 纳米焊丝更适用于 2195 铝锂合金。

参 考 文 献

[1] 陈丹, 刘婷, 赵艳秋, 等. 晶粒尺寸对双激光束双侧同步焊接接头力学性能的影响[J]. 中国激光, 2021, 48(10): 1002120.
Chen D, Liu T, Zhao Y Q, et al. Effect of grain size on mechanical properties of double laser-beam bilateral synchronous welding joint[J]. Chinese Journal of Lasers, 2021, 48(10): 1002120.

[2] Nayan N, Murty S N, Jha A K, et al. Processing and characterization of Al-Cu-Li alloy AA2195 undergoing scale up production through the vacuum induction melting technique[J]. Materials Science and Engineering: A, 2013, 576: 21-28.

[3] 雷正龙, 毕思源, 张新瑞, 等. 2195 铝锂合金 T 型接头双侧激光摆动焊接组织与性能分析[J]. 中国激光, 2022, 49(8): 0802003.
Lei Z L, Bi S Y, Zhang X R, et al. Microstructure and mechanical properties of double-sided laser swing welding of 2195 Al-Li alloy T-joints[J]. Chinese Journal of Lasers, 2022, 49(8): 0802003.

[4] Sun Z Y, He B, Li K J, et al. Study on microstructure evolution and aging precipitation behavior of a novel Al-Li alloy fabricated by laser rapid melting[J]. Journal of Alloys and Compounds, 2022, 908: 164630.

[5] Rioja R J, Liu J. The evolution of Al-Li base products for aerospace and space applications[J]. Metallurgical and Materials Transactions A, 2012, 43(9): 3325-3337.

[6] Williams J C, Jr, Starke J. Progress in structural materials for aerospace systems[J]. Acta Materialia, 2003, 51(19): 5775-5799.

[7] Rioja R J. Fabrication methods to manufacture isotropic Al-Li alloys and products for space and aerospace applications[J]. Materials Science and Engineering: A, 1998, 257(1): 100-107.

[8] Zhang Z F, Huang Y M, Qin R, et al. XGBoost-based on-line prediction of seam tensile strength for Al-Li alloy in laser welding: experiment study and modelling[J]. Journal of Manufacturing Processes, 2021, 64: 30-44.

[9] 李桓, 徐光霈, 张宇辉, 等. 2219/5A06 异种铝合金焊接接头组织与性能相关性[J]. 焊接学报, 2020, 41(9): 8-15, 97.
Li H, Xu G P, Zhang Y H, et al. Correlation between microstructure and properties of 2219/5A06 dissimilar aluminum alloy welded joint[J]. Transactions of the China Welding Institution, 2020, 41(9): 8-15, 97.

[10] 陈永来, 李劲风, 张绪虎, 等. 2195 铝锂合金摩擦搅拌焊接头组织[J]. 中国有色金属学报, 2016, 26(5): 964-972.
Chen Y L, Li J F, Zhang X H, et al. Structure of friction-stir welding joint of 2195 Al-Li alloy[J]. The Chinese Journal of Nonferrous Metals, 2016, 26(5): 964-972.

[11] Yang Z B, Zhao X, Wang T, et al. Effects of keyhole status on melt flow and flow-induced porosity formation during double-sided laser welding of AA6056/AA6156 aluminium alloy T-joint[J]. Optics & Laser Technology, 2019, 109: 39-48.

[12] Cao X, Wallace W, Immarigeon J P, et al. Research and progress in laser welding of wrought aluminum alloys. II. metallurgical microstructures, defects, and mechanical properties[J]. Materials and Manufacturing Processes, 2003, 18(1): 23-49.

[13] Liu T, Zhao Y Q, Kang Y, et al. Effect of micro morphology in different zones on mechanical properties of 2060 Al-Li alloy laser welded joints[J]. Journal of Manufacturing Processes, 2020, 50: 336-344.

[14] 张心怡. 2060 铝锂合金激光焊接组织及力学性能研究[D]. 北京: 北京工业大学, 2016.
Zhang X Y. Microstructures and mechanical properties of laser

welded joints of 2060 aluminum lithium alloy[D]. Beijing: Beijing University of Technology, 2016.

[15] 刘强 . 活性激光焊接对铝合金焊缝气孔及合金元素烧损的影响[D]. 镇江: 江苏科技大学, 2016.
Liu Q. Effect of activating laser welding on porosity of aluminum welding and alloys elements burning[D]. Zhenjiang: Jiangsu University of Science and Technology, 2016.

[16] 林凯莉, 杨武雄, 吕俊霞, 等 . 2198-T851 铝锂合金激光焊接工艺研究[J]. 中国激光, 2014, 41(1): 0103007.
Lin K L, Yang W X, Lü J X, et al. Laser beam welding study of 2198-T851 aluminum-lithium alloy[J]. Chinese Journal of Lasers, 2014, 41(1): 0103007.

[17] 栗卓新, 田振, 李红, 等 . 纳米陶瓷颗粒对铝合金焊缝强度和微观组织影响的研究进展[J]. 材料导报, 2022, 36(1): 141-148.
Li Z X, Tian Z, Li H, et al. Research progress on the influence of nanoparticles on weld strength and microstructure of aluminum alloy[J]. Materials Reports, 2022, 36(1): 141-148.

[18] Li Y, Zhao Y Q, Wang J Y, et al. Effect of laser power on the grain morphology and microhardness of dual laser-beam bilateral synchronous welded 2219 aluminium alloy T-joint[J]. Science and Technology of Welding and Joining, 2021, 26(7): 540-550.

[19] Jin P, Liu Y B, Li F X, et al. Realization of synergistic enhancement for fracture strength and ductility by adding TiC particles in wire and arc additive manufacturing 2219 aluminium alloy[J]. Composites Part B: Engineering, 2021, 219: 108921.

[20] Zhang M F, Han Y F, Jia C B, et al. Improving the microstructures and mechanical properties with nano-Al_2O_3 treated wire in underwater submerged arc welding[J]. Journal of Manufacturing Processes, 2022, 74: 40-51.

Influence of Nanoparticles on Laser Weld Microstructure of 2195 Al-Li Alloy

Zhan Xiaohong[1*], Li Yue[1], Zhao Yanqiu[1], Wang Jianfeng[1], Gao Xuesong[2], Zhou Jun[2]

[1]*College of Materials Science and Technology, Nanjing University of Aeronautics and Astronautics, Nanjing* 211106, *Jiangsu, China*;

[2]*Nanjing Institute of Advanced Laser Technology, Nanjing* 211106, *Jiangsu, China*

Abstract

Objective High-strength 2195 aluminum-lithium (Al-Li) alloy exhibits excellent strength and fracture toughness both at room and low temperatures and is mainly used in the cryogenic storage tanks of space launch vehicles to satisfy the weight reduction requirements of key structures in the aerospace sector. Laser welding technology is a high-energy beam connection method with high energy density, good welding quality, high precision, high production efficiency, significant weight reduction, and other characteristics. Laser welding is an ideal joining technology for spacecraft tank structures. Alloying elements influence the type, size, volume fraction, and distribution pattern of precipitates in aluminum alloys, while precipitates and microstructures determine the mechanical properties of these alloys. Therefore, optimizing the composition of welded joints fabricated from 2195 Al-Li alloy can considerably improve the joint properties. In this study, 4047 filler wires and 2319 filler wires are used to conduct laser welding experiments on 2195 Al-Li alloy to compare and analyze the effects of different filler elements on the microstructure, alloy element distribution, and mechanical properties of laser-welded joints.

Methods The dimensions of welded parts used in this work were 100 mm×50 mm×2 mm (Fig. 1). The utilized wires included 4047 filler wires with a diameter of 1.2 mm and 2319 filler wires with 2% (mass fraction) TiC particles. Al-Li alloy laser fillet welding was performed using a laser. Laser welding was conducted with a 6-axis robot, and the welded specimens were clamped using a special welding fixture. Wire-filling welding was performed using a wire feeder. Scanning electron microscopy (SEM) was conducted to observe the microstructure of the joint cross-section and tensile fracture morphology. The obtained tissue morphology was utilized to study the microstructural characteristics of joints with different welding wires and their tensile fracture mechanism. Chemical compositions of different areas in joint cross-sections were characterized by energy-dispersive X-ray spectroscopy (EDS) to determine elemental distributions and their influence on the joint properties.

Results and Discussions Laser self-melting welding and laser welding with 4047 filler wire produce the microstructure with a fusion line passing close to the equiaxial fine crystal zone (EQZ), columnar crystal zone, and central dendrite zone (Figs. 4 and 5). The presence of EQZ near the fusion line is caused by the presence of Zr and Li elements in the alloy. The laser wire filling welding using 2319 significantly improves the properties of the welding seam (Fig. 6) containing fine equiaxial crystals owing to the addition of TiC particles to the center of the melt pool. This increases the number of nucleation centers and substantially compresses the growth space for columnar crystals, thus promoting the transformation of columnar branch crystals to equiaxial crystals. Grain boundary segregation and elemental burnout strongly influence the weld, leading to the redistribution of its elements and accumulation of Cu atoms at the grain boundaries (Tables 2-5). The 2195 aluminum-lithium alloy laser-welded joints undergo significant softening with a reduction in the number of strengthening phases due to the strong lithium and copper elemental burnout in the weld area and significant strength loss without wire filling. After wire filling, the mechanical properties of the joint are significantly improved owing to the refinement of weld grains and increase in the number of weld strengthening phases. In particular, using 4047 wires as a filler considerably increases the tensile strength of the laser-welded joints produced from 2195 aluminum-lithium alloy (Fig. 11).

Conclusions The self-melting welding joint of 2195 aluminum-lithium alloy and joint by laser wire filling welding with 4047 consist of equiaxed fine crystals, columnar crystals, and equiaxed dendritic crystals. The laser wire filling welding joints using 2319 consist of equiaxed fine crystals and equiaxed dendritic crystals. In contrast to laser self-melting welding, the weld by laser wire filling welding using 2319 contains a large fraction of Cu atoms distributed at the grain boundaries with a Cu element supplementation rate of 6.5%. After 4047 wire filling, the 2195 aluminum-lithium alloy laser welding process is supplemented with Si atoms; the weld tissue grain boundaries contain a large number of Si atoms, and the Si phase strengthening effect is enhanced. Compared with laser self-melting welding, laser filler welding is more energetically intense, and its Li element burnout is more significant. Both 4047 filler wires and 2319 filler wires increase the tensile strength of the laser-welded joints fabricated from 2195 aluminum-lithium alloy with a stronger effect observed for the 4047 filler wires. As a result, the tensile strength of the 2195 Al-Li alloy laser-welded joints is 14.19% higher than that of the joints produced via laser self-melting welding.

Key words laser technique; laser welding; aluminum-lithium alloy; fine equiaxed grains; nano-welding wire; microstructure